

A new modelling approach based on Binary Model and X-FEM to investigate the mechanical behaviour of textile reinforced composites

G. Haasemann¹, M. Kästner² and V. Ulbricht³

Abstract: The purpose of this paper is the presentation of a new efficient modelling strategy based on the combination of Binary Model and Extended Finite Element Method (X-FEM). It is applied to represent the internal architecture of textile reinforced composites where the resin-saturated fabric is characterised by a complex geometry. Homogenisation methods are used to compute the effective elastic material properties. Thereby, the discrete formulation of periodic boundary conditions is adapted regarding additional degrees of freedom used by finite elements which are based on the X-FEM. Finally, the results in terms of effective material properties reveal a good agreement with parameters obtained by experimental tests.

Keywords: Composite materials, Binary Model, X-FEM, Homogenisation method.

1 Introduction

The material design process for novel textile reinforced composites requires an integrated simulation of the material behavior and estimation of the effective properties used in a macroscopic structural analysis. Due to the high anisotropy, a large number of parameters are necessary to formulate the macroscopic constitutive relations. Therefore, the determination of these parameters based on experimental tests is very expensive. However, the homogenisation method applied to composites provides a less laborious approach [Haasemann, Kästner, and Ulbricht (2006); Pahr and Böhm (2008); Takashima, Nakagaki, and Miyazaki (2007)]. Here, the basic principle is the consideration of the composite at different scales. At the macro-scale we assume the material to be homogeneous. The homogenisation method gives the mathematical foundation for the transition between the material behaviour

¹ TU-Dresden, Germany, email: georg.haasemann@tu-dresden.de.

² TU-Dresden, Germany, email: markus.kaestner@tu-dresden.de.

³ TU-Dresden, Germany, email: volker.ulbricht@tu-dresden.de.

at the heterogeneous meso- or micro-scale and the macro-scale. This comprises the definition of a representative volume element (RVE) which includes the identification of the inner topology. Furthermore, all mechanical properties of fibre and matrix material are needed. The FEM provides the most flexible approach to solve the mechanical boundary value problem defined by the homogenisation theory in conjunction with the RVE-model.

Depending on the geometric complexity of the textile reinforcement, the preparation of the RVE-model becomes a time-consuming task. This motivates the development of new improved modelling techniques which are characterised by (i) a high efficiency, (ii) reduced computational effort and (iii) an automated model generation. In this context, Section 2 contains a survey of conventional and advanced modelling techniques, namely the Binary Model and the Extended Finite Element Method (X-FEM).

One intention of this work is the development of a modelling technique, which is improved regarding the application to composites consisting of polymer matrix material and biaxial weft-knit made of glass fibres. Fig. 1 illustrates the general composition of a biaxial weft-knitted fabric.

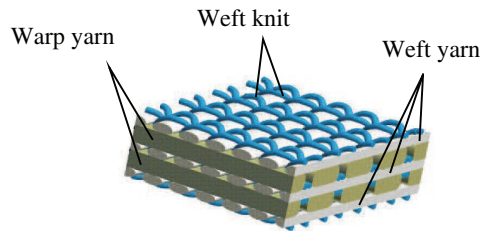


Figure 1: Biaxial weft-knit

The use of this textile reinforcement is beneficial to the effective material properties. For instance a high in-plane stiffness is assured by the biaxial warp- and weft-yarns. Furthermore, the weft-knitted structure prevents the composite from delamination and provides an improved out-of-plane stiffness.

The fabric incorporates multiple yarn types with significantly different cross-sections. This fact causes difficulties during the mesh generation. As shown in Section 3, the combination of Binary Model and X-FEM provides a new approach which avoids these problems and unifies the advantages of both modelling techniques.

In Section 4, the basic principle as well as the essential equations of the homogenisation method are summarised. In order to solve the resulting boundary value prob-

lem based on the FEM, a discrete formulation of boundary conditions is needed. For this purpose, an extended finite element model requires special considerations which are given in this section as well.

Finally in Section 5 the new modelling approach is applied to a polymer composite material reinforced by a biaxial weft-knitted fabric. A comparison with experimental test data will show the accuracy of the numerical results.

2 FE-Modelling techniques

In most applications, the structure of the composite material can be considered as shells or plates, e.g. the macroscopic shape is rather two- than three-dimensional. However, a closer observation of many composite materials, for instance the one considered in this paper, reveals a distinct spatial internal topology at the meso-scale. Therefore, a FE-representation of the RVE necessitates the use of volume elements.

In general, conventional volume elements with linear or quadratic shape functions are applied to generate RVE-models [Galli, Botsisb, and Janczak-Rusch (2008); Huang and Chiu (2008)]. As illustrated in Fig. 2, this modelling procedure requires the alignment of element boundaries to the material interfaces.

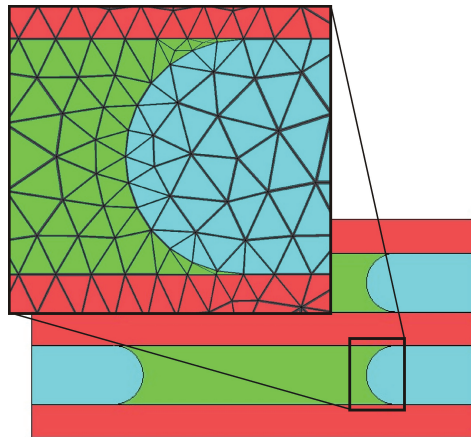


Figure 2: Conventional mesh

Then the application to complex structured reinforcements becomes time-consuming and causes a large number of finite elements which increases the computational effort. As it can be clearly seen in Fig. 2, the danger of generating bad-shaped

elements becomes potentially high. This may produce a poor convergency and incorrect results.

Up to now, alternative modelling techniques have been developed. In general, they are specialised in application to a specific group of composite materials. For example, Rolfes, Ernst, Hartung, and Teßmer (2006) have shown the successful application of the voxel approach to unidirectional fibre reinforced materials. Furthermore, the infinite element method introduced by Liu, Chen, and Chiou (2005) is used to investigate effective material properties of particle reinforced composites. A multitude of available publications concerning the meshless analysis of non-homogeneous solids shows the high potential of this sophisticated method [Hagihara, Tsunori, Ikeda, and Miyazaki (2007); Dang and Sankar (2008); Long, Liu, and Li (2008)].

The development in this paper is based on the Binary Model and the X-FEM. Subsequently, both techniques which are adapted for the efficient modelling of complex structured fibre reinforced materials will be described.

2.1 Extended finite element method

Based on the partition of unity method, the X-FEM allows for a representation of certain field discontinuities inside a finite element [Melenk and Babuska (1996)]. First applications of this powerful method were related to the modelling of cracks and crack propagation without the need of re-meshing [Moës, Dolbow, and T. (1999); Stazi, Budyn, Chessa, and Belytschko (2003)]. Currently, this technique is also used to represent a micro-structure with complex geometry and even to perform coupled atomistic-continuum simulations [Moës, Cloirec, Cartraud, and Remacle (2003); Haasemann, Kästner, and Ulbricht (2006); Ulbricht, Kästner, Lichtenekert, Brummund, Modler, Hufenbach, Böhm, Ebert, Grüber, Langkamp, and Lepper (2008); Kästner and Ulbricht (2006); Kästner, Haasemann, Brummund, and Ulbricht (2008); Chirputkar and Qian (2008)].

In the following, a two-dimensional model as shown in Fig. 3a will be used to explain and demonstrate the fundamental principle of the X-FEM.

The geometry conforms to a unit cell of a unidirectional (UD) fibre reinforced composite. Due to the alignment of element boundaries to the material interface, a conventional FE-Mesh as given in Fig. 3b evince the typical non-regular shaped elements.

Extending the approximation of the classical displacement field \mathbf{u} by an enrichment, the X-FEM enables us to model the discontinuity surface based on a regular mesh (Fig. 4a).

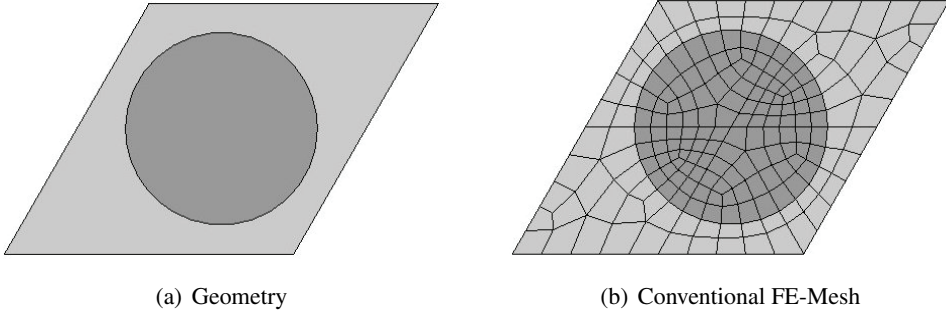


Figure 3: Unit cell of a UD-composite

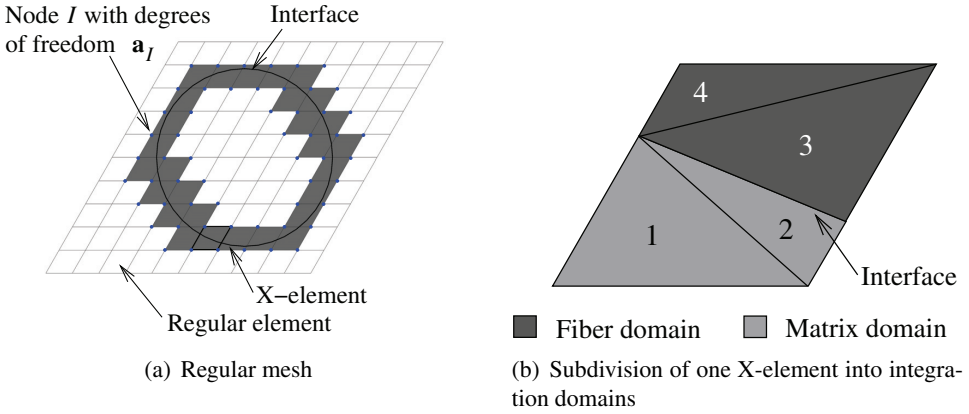


Figure 4: Model generation based on the X-FEM

In general, the enriched displacement field is given by

$$\mathbf{u}(\boldsymbol{\xi}) = \sum_I N_I(\boldsymbol{\xi}) \mathbf{u}_I + \sum_I N_I(\boldsymbol{\xi}) \mathbf{a}_I F(\boldsymbol{\xi}) \quad , \quad (1)$$

where the first part, denoting the linear approximation, consists of the shape functions N_I depending on the local coordinates $\boldsymbol{\xi}$ and displacement values \mathbf{u}_I at node I . The formulation of the enrichment, i.e. the second part in Eq. (1), is based on additional degrees of freedom (dof) \mathbf{a}_I and the enrichment function F . Depending on the type of discontinuity, there are several possibilities to define the function F . Here, the intention lies in the modelling of heterogeneous materials. Besides the local change of material properties, an arbitrary deformation may cause a discontinuous strain and stress field at the material interface. This can be achieved

using the following definition, which was proposed by Moës, Cloirec, Cartraud, and Remacle (2003).

$$F(\boldsymbol{\xi}) := \sum_I N_I |\varphi_I| - \left| \sum_I N_I \varphi_I \right| \quad (2)$$

This formulation includes values of the level-set function $\varphi_I := \varphi(\boldsymbol{\xi}_I)$ at the location $\boldsymbol{\xi}_I$ of element nodes. As can be seen in the following equation, the level-set function corresponds to the signed distance between any location $\boldsymbol{\xi}$ inside the element domain and the closest point at the interface $\bar{\boldsymbol{\xi}}$ [Wang, Lim, Khoo, and Wang (2007)].

$$\varphi(\boldsymbol{\xi}) := \min \left| \boldsymbol{\xi} - \bar{\boldsymbol{\xi}} \right| \text{sign} \left[(\boldsymbol{\xi} - \bar{\boldsymbol{\xi}}) \cdot \mathbf{n} \right] \quad (3)$$

In Eq. (3), \mathbf{n} denotes a unit normal vector at the interface.

The choice of the enrichment function according to Eq. (2) assures the following properties:

- Representation of discontinuities in the strain and stress field,
- Unaffected displacement field continuity and
- Restriction of the displacement field enrichment to elements which include a part of the interface.

Due to the last aspect, only those nodes in Fig. 4a marked by a blue dot require additional dof \mathbf{a}_I . Finally, the mesh can be subdivided into so called X-elements and ordinary finite elements.

A derivation of FE-equations requires a subdivision of the considered domain Ω into regions Ω_e occupied by finite elements. The virtual work principle in conjunction with the approximation of the displacement field by Eq. (1) leads to the equilibrium equations $\mathbf{K}\mathbf{u} = \mathbf{f}$, where \mathbf{f} is the load vector and the stiffness matrix \mathbf{K} can be expressed by

$$\mathbf{K} = \bigcup \int_{\Omega_e} \mathbf{B}^T \mathbf{D} \mathbf{B} d\Omega \quad . \quad (4)$$

The symbol \cup denotes the assembly of all element matrices and the matrix \mathbf{B} defines the transformation between strain $\boldsymbol{\varepsilon}$ and all dof, i.e. displacement dof \mathbf{u} as well as additional dof \mathbf{a} . Since the material stiffness matrix \mathbf{D} depends on the location inside the element domain and \mathbf{B} represents a discontinuous strain distribution, the numerical evaluation of the integral in Eq. (4) requires special attention. For that

purpose, the element sub-domains defined by the material interface are subdivided again into triangle- or tetrahedral-shaped regions Ω_S for 2D- or 3D-elements, respectively. As an example, Fig. 4b shows the triangulation of the element which is bordered with a thick line in Fig. 4a. Using the integration stations of these sub-domains Ω_S allows for a numerical integration procedure which accounts for the discontinuity in \mathbf{C} and \mathbf{B} since each triangle or tetrahedron has a unique correlation to the underlying material. In the example, triangle 1 and 2 are assigned to the matrix material and triangle 3 and 4 belong to the fibre material.

2.2 Binary Model

The Binary Model provides a very efficient approach to model composites with highly complex textile reinforcement. It was first introduced by Carter, Cox, and Fleck (1994) to simulate the mechanical behavior of through-the-thickness angle interlock woven composites. Further development and application have been reported in modelling failure due to broken fibres and simulation of the dynamic behaviour [Xu, Cox, McGlockton, and Carter (1995); McGlockton, Cox, and McMeeking (2003); Haasemann (2003)].

In a first step of generating the Binary Model, the mechanical properties of a fibre reinforced composite are subdivided as follows:

- The axial stiffness of all yarns are represented by tows,
- All other properties of matrix material and the transverse stiffness of fibres and Poisson's effects are assigned to the so called effective medium.

This separation requires a significant difference between the stiffness of fibre and matrix material. As a result of this step we have a region, which is equivalent to the volume of the composite, occupied by the effective medium. Superimposed tow-lines run along the center of each yarn. The next modelling step comprises the transition of this Binary Model into a FE-Model.

As shown in Fig. 5, this leads to a regular mesh of volume elements representing the effective medium combined with line elements mapping the characteristics of all tows.

As reported by Xu, Cox, McGlockton, and Carter (1995), the computation of all elastic parameters to be assigned to line and volume elements is based on material properties of the composite constituents, i.e. matrix and fibre. Considering a composite which is dominated by orthogonal aligned fibres, the anisotropic elastic properties of the effective medium can be estimated using an analytical model of an unidirectional composite [Cox and Dadkhah (1995)]. With respect to the coordinate

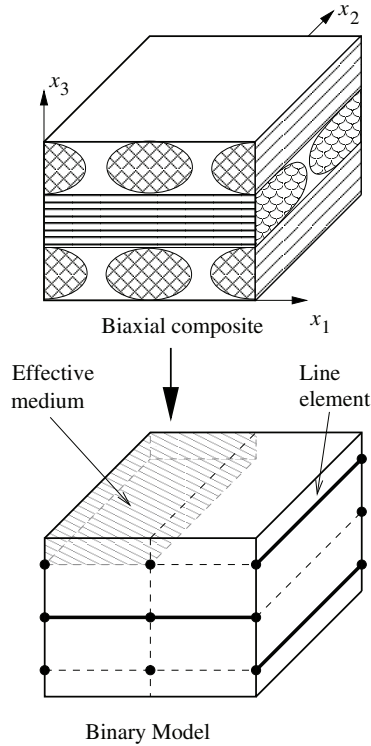


Figure 5: Binary Model

system given in Fig. 5, this leads to the following relations, where the superscripts (em) and (ud) refer to effective medium and UD-composite, respectively.

$$\begin{aligned}
 E_1^{(em)} &= E_2^{(em)} = 2(1 + \nu_{xy}^{(ud)})G_{xy}^{(ud)} \\
 E_3^{(em)} &= E_y^{(ud)} \\
 \nu_{13}^{(em)} &= \nu_{23}^{(em)} = \nu_{xy}^{(ud)} \\
 \nu_{12}^{(em)} &= \nu_{xy}^{(ud)} \\
 G_{12}^{(em)} &= G_{xy}^{(ud)} \\
 G_{13}^{(em)} &= G_{23}^{(em)} = G_{xy}^{(ud)}
 \end{aligned} \tag{5}$$

Local coordinates (x, y, z) with fibres aligned to the x -axis are used to define all UD-parameters in equation (5).

Finally, the rule-of-mixture gives the effective Young's modulus of tows

$$E_t = E_m + v_f(E_f + E_m) \quad , \quad (6)$$

where v_f is the fibre volume fraction and E_m, E_f the Young's moduli of fibre and matrix material, respectively. Since tows and effective medium are superimposed to each other, the Young's modulus of line elements is derived as

$$E_l = E_t - E_{em} \quad (7)$$

with E_{em} denotes the Young's modulus of the underlying effective medium. Eq. (7) avoids a multiple consideration of the matrix material.

2.3 Comparison of X-FEM and Binary Model

In general, a FE-mesh representing the architecture of a composite with biaxial weft-knit reinforcement can be generated based on the X-FEM as well as on the Binary Model. However, besides all beneficial properties, both modelling strategies exhibit different disadvantages which will be outlined subsequently.

Although the Binary Model provides a very convenient concept for representing even highly complex structured yarns, it does not account explicitly for the behaviour at the interface between yarn and matrix regions. Instead, the effective medium is used to describe the influence of geometry and material properties only implicitly. This requires the derivation of constitutive equations such as given in Eq. (5). A further application of the Binary Model to include material nonlinearities such as plasticity and viscosity requires suitable approximations of these properties. As already investigated by the authors, there is no solution to this task which is as straightforward as in the case of linear elasticity.

Applying the X-FEM to fibre reinforced composites avoids these difficulties since all material interfaces are represented explicitly based on the enrichment in Eq. (1). But new problems arise from modelling different yarns with significantly different dimensions of the cross sections. For example, the diameters of weft-knit and warp-yarn are approximately 0.1 mm and 3.0 mm, respectively. Since the interpolation of the material interface inside one X-element is basically linear, at least 2×2 or better 3×3 elements are necessary to model the cross-section of the weft-knit. In order to retain a regular mesh, the number of elements used for the entire unit cell becomes extremely high. In view of modelling the warp- and weft-yarn, the element size, limited due to the small cross-section of the weft-knit, is unnecessarily small. This aspect motivates the development of a modelling strategy which combines X-FEM and Binary Model.

3 Combination of X-FEM and Binary Model

The comparison in Section 2.3 shows that the Binary Model is the most efficient way to represent the complex geometry of weft-knits whereas the X-FEM proves its superiority for modelling the weft- and warp-yarns. Thus, we are incorporating both modelling techniques in one FE-model. With respect to the composite material considered in this paper, line elements are used to model the geometry of all weft-knits and X-elements contain the interfaces between warp- and weft-yarns. As summarized in Tab. 1, all elements which are not cut by the material interfaces remain ordinary finite elements.

Table 1: Finite element representation

Composite component	Element type
Weft-knit	Line elements
Interface between warp- and weft-yarns	X-elements
Domain without material interfaces	Ordinary elements

With this combination of both modelling strategies all advantageous properties are unified.

The following considerations concern the integration of line elements into an existing mesh of ordinary and extended volume elements. In general, all nodes of line and volume elements are merged, i.e. the number of global dof is determined by the number of volume element nodes only. With respect to the geometry of the weft-knit, this restriction on placing line element nodes causes either very small-sized or non-regular shaped volume elements.

In order to avoid these unfavourable consequences, we account for the case of positioning such nodes inside a volume element. Then, a multiple point constrain (MPC) is used to enforce compatibility between the displacement field inside the volume element and the displacements $\{\mathbf{u}_i\}_{line}$ of the so call MPC-node i . As shown in Fig. 6, the location of such MPC-node is given by the local coordinates $\boldsymbol{\xi}^t = \{\xi_1^t, \xi_2^t, \xi_3^t\}^T$.

In the case of an X-element with the dof-vector $\{\mathbf{u}_I \mathbf{a}_I\}_x^T$ of node I , a MPC leads to

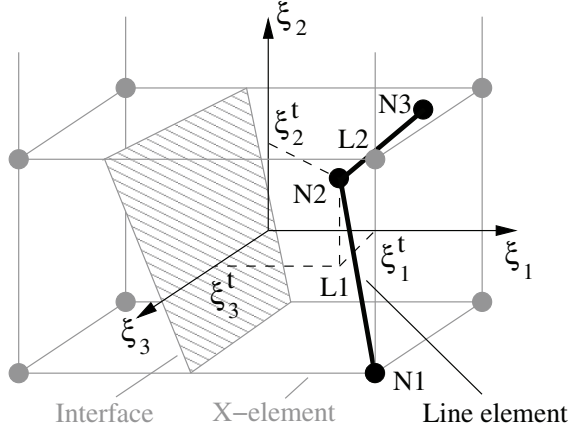


Figure 6: Combination of X-elements with line elements

the equations

$$\{\mathbf{u}_i\}_{line} = \sum_{I=1}^8 [\mathbf{T}_I(\boldsymbol{\xi}^t)] \left\{ \begin{array}{c} \mathbf{u}_I \\ \mathbf{a}_I \end{array} \right\}_x \quad (8)$$

where the matrix $[\mathbf{T}_I]$ is given by

$$[\mathbf{T}_I] = \begin{bmatrix} \bar{N}_I & 0 & 0 & \bar{N}_I \bar{F}_I & 0 & 0 \\ 0 & \bar{N}_I & 0 & 0 & \bar{N}_I \bar{F}_I & 0 \\ 0 & 0 & \bar{N}_I & 0 & 0 & \bar{N}_I \bar{F}_I \end{bmatrix} . \quad (9)$$

In Eq. (9), $\bar{N}_I := N(\boldsymbol{\xi}^t)_I$ and $\bar{F}_I := F(\boldsymbol{\xi}^t)_I$ are the shape functions and enrichment functions, respectively, evaluated at the location $\boldsymbol{\xi}^t$. Defining a vector $\{\mathbf{u}\}_x$ which contains all dof of the X-element, Eq. (8) can be replaced by

$$\{\mathbf{u}_i\}_{line} = [\bar{\mathbf{T}}(\boldsymbol{\xi}^t)] \{\mathbf{u}\}_x \quad , \quad (10)$$

where the matrix $[\bar{\mathbf{T}}]$ is composed of values given in Eq. (9) for all nodes $I \in \{1, \dots, 8\}$.

Since both nodes of one line element are not necessarily MPC-nodes, we have to distinguish between two combinations. In the first case which is illustrated in Fig. 6 by line element L1, the dof of one node can be merged with the dof \mathbf{u}_1 of volume element node N1. The final transformation can be expressed by

$$\{\mathbf{u}\}_{line} = \begin{bmatrix} \mathbf{I} & \mathbf{0} \\ \mathbf{0} & \bar{\mathbf{T}}_2 \end{bmatrix} \left\{ \begin{array}{c} \mathbf{u}_1 \\ \mathbf{u}_x \end{array} \right\} \quad , \quad (11)$$

where \mathbf{I} is the identity matrix and $\{\mathbf{u}\}_{line}$ - the dof of the line element. The subscript of $\bar{\mathbf{T}}_2$ refers to the node number.

The line element L2 in Fig. 6 represents the second case, where all dof of both nodes, which are located beside the nodes of volume elements, are treated by MPC. Then the displacement continuity is achieved by the equation

$$\{\mathbf{u}\}_{line} = \begin{bmatrix} \bar{\mathbf{T}}_2 \\ \bar{\mathbf{T}}_3 \end{bmatrix} \{\mathbf{u}\}_x . \quad (12)$$

Denoting the matrices in Eq. (11) and (12) by $[\mathbf{T}]$, the stiffness matrix $[\mathbf{k}]_L$ of the line element is transformed by

$$[\mathbf{T}]_{Lgl} = [\mathbf{T}]^T [\mathbf{k}]_L [\mathbf{T}] . \quad (13)$$

Note that the resulting matrix $[\mathbf{T}]_{Lgl}$ addresses only dof of volume elements, i.e. the number of global dof is not changed due to the existence of line elements.

The numerical implementation of these MPC requires further differentiation since e.g. the two nodes of one line element may be placed in two adjacent volume elements or the types of the underlying volume elements are different. However, as the specific relations can be derived based on the equation given before, these cases are not detailed here.

4 Homogenisation Method

4.1 Basic equations of the homogenisation method

Homogenisation methods are widely used in order to estimate macroscopic or effective material properties and to replace any heterogeneous material by a homogeneous equivalent medium. There is a number of approaches which are based on different assumptions and requirements [Hollister and Kikuchi (1992); Pierard (2006)]. Furthermore, these methods can be classified into analytically or numerically solved problems. Since the first one can not deal with complex fabric architectures, we are using a systematic mathematical approach which is based on the energy equivalence [Hill (1963)]. The resulting boundary value problem can be solved by numerical methods such as the FEM. In the following, the basic assumptions and equations of this homogenisation are summarised.

First of all, a scale separation is required to clearly identify the level of a homogeneous and heterogeneous material, respectively. Certainly, a structure made of composite material having the characteristic length L is assigned to the macroscopic level. Regarding the textile reinforced material, we will furthermore distinguish between a meso- and micro-scale. Thereby, the geometry of the fabric architecture

with the characteristic length l belongs to the meso-structure where the domain of a yarn embedded in matrix material is considered to be homogeneous. The next finer resolution belongs to the micro-level which then shows a small collection or even just a single fibre inside the yarn and its surrounding matrix. For the derivation of relations between quantities defined at two different scales, a representative volume element of volume V and surface A covering the heterogeneous domain $Y = \{\vec{\mathbf{y}} = y^i \vec{\mathbf{e}}^i, |y^i| < \frac{a}{2}\}$ is defined. Since the textile geometry can be considered as a periodic array of identical patterns, the domain of the RVE conforms to a unit cell. In order to consider the macroscopic structure as homogeneous, the following relation

$$L \gg a \gg l \quad (14)$$

between the characteristic measures must be required. Considering the respective lengths, this relation is valid for the homogenisation at the micro-scale, too.

The volume average

$$\mathbf{F} := \langle \mathbf{f}(\mathbf{y}) \rangle = \frac{1}{V} \int_Y \mathbf{f}(\mathbf{y}) dV \quad (15)$$

is used to link any physical quantity $\mathbf{f}(\mathbf{y})$ at the heterogeneous configuration to the respective homogeneous value \mathbf{F} . In case of the small strain tensor, this leads to the relation

$$\mathbf{E} = \frac{1}{V} \int_{\partial Y} (\mathbf{u} \otimes \mathbf{n})_s dA \quad , \quad (16)$$

where \mathbf{u} is the displacement vector, \mathbf{n} - the unit normal vector, ∂Y - the domain of the RVE surface and $(\)_s$ is used to denote a symmetry operation on the enclosed tensor.

Applying Eq. (15) to the heterogeneous stress field $\boldsymbol{\sigma}(\mathbf{y})$ leads to the relations

$$\boldsymbol{\Sigma} := \langle \boldsymbol{\sigma}(\mathbf{y}) \rangle = \frac{1}{V} \int_{\partial Y} \mathbf{t} \otimes \mathbf{y} dA \quad (17)$$

with the vector of surface traction $\mathbf{t} := \boldsymbol{\sigma} \cdot \mathbf{n}$. Furthermore, the absence of body forces is presumed to derive the expression based on the surface integral. Note that Eq. (16) as well as (17) show, that the specification of respective boundary values suffice to gain a specific macroscopic strain or stress state.

In order to solve the mechanical field equations, boundary conditions are required. These can be obtained based on the Hill-Mandel lemma

$$\boldsymbol{\Sigma} : \mathbf{E} = \langle \boldsymbol{\sigma}(\mathbf{y}) \rangle : \langle \boldsymbol{\varepsilon}(\mathbf{y}) \rangle \quad . \quad (18)$$

It can be shown, that the following formulations of boundary conditions satisfy this energy equivalence.

- Linear displacements $\mathbf{u}(\mathbf{y}) = \mathbf{E} \cdot \mathbf{y}$,
- Constant tractions $\mathbf{t}(\mathbf{y}) = \mathbf{\Sigma} \cdot \mathbf{n}(\mathbf{y})$ and
- Periodic displacements $\mathbf{u}(\mathbf{y}^+) - \mathbf{u}(\mathbf{y}^-) = \mathbf{E} \cdot (\mathbf{y}^+ - \mathbf{y}^-)$ and anti-periodic tractions $\mathbf{t}(\mathbf{y}^+) = -\mathbf{t}(\mathbf{y}^-)$.

Here, two coordinates denoted by the superscript $+$ and $-$ refer to associated points at opposed surfaces.

In general, the results computed with periodic boundary conditions and anti-periodic tractions have the best agreement to experimental data. Hence, the following analysis will be focused on the discrete formulation of these boundary conditions regarding X-elements.

The general approach to compute the macroscopic linear elastic material tensor \mathbf{C} based on periodic boundary conditions can be described as follows:

1. Generating a FE-model of the RVE which represents the inner architecture of the composite material,
2. Applying periodic boundary conditions where one component of \mathbf{E} is one, e.g. $E_{KL} = 1$, and all remaining strain components are zero,
3. Solving the boundary value problem and
4. Computing the macroscopic stress $\mathbf{\Sigma}(E_{KL})$ according to equation (17).

Since we have chosen $E_{KL} = 1$, the macroscopic stress corresponds to $C_{ijkl} = \Sigma_{ij}(E_{KL})$. From this relation it follows, that the computation of the entire macroscopic material tensor \mathbf{C} requires the solution of all six unit-deformations.

4.2 Periodic boundary conditions and X-FEM

A solution of the homogenisation problem with FEM requires the discrete formulation of boundary conditions based on degrees of freedom (dof). To improve the modelling efficiency, it is reasonable to introduce a vector $\Delta \mathbf{y}^\alpha := \mathbf{y}^{\alpha+} - \mathbf{y}^{\alpha-}$, $\alpha \in \{1, 2, 3\}$ where α is the pair number of surfaces. So this consideration are limited to RVE's with 6 surfaces. However, they can have any shape and orientation. The only restriction comes from the geometric periodicity in what follows that $\Delta \mathbf{y}^\alpha = \text{const}$. Using $\Delta \mathbf{y}^\alpha$ to describe periodic displacements leads to the equation

$$\Delta \mathbf{u}^\alpha = \mathbf{E} \cdot \Delta \mathbf{y}^\alpha \quad (19)$$

with $\Delta \mathbf{u}^\alpha := \mathbf{u}(\mathbf{y}^{\alpha+}) - \mathbf{u}(\mathbf{y}^{\alpha-})$. These generalised displacements $\Delta \mathbf{u}^\alpha$ are independent of \mathbf{y} which motivates the definition of three master nodes in the FE-Model, each associated to the surface pair α . Then, the displacements of respective nodes of the RVE-model are linked to the associated master node according to the periodic boundary conditions. Finally, the displacement values computed by Eq. (19) are assigned.

To account for nodes at the surface mesh belonging to an X-element, it is required to derive boundary conditions which have to be applied to additional dof \mathbf{a}_j . As illustrated in Figure 7, we have to distinguish between two cases, depending on whether the material interface inside an X-element (i) penetrates the unit cell surface or (ii) remains inside the unit cell.

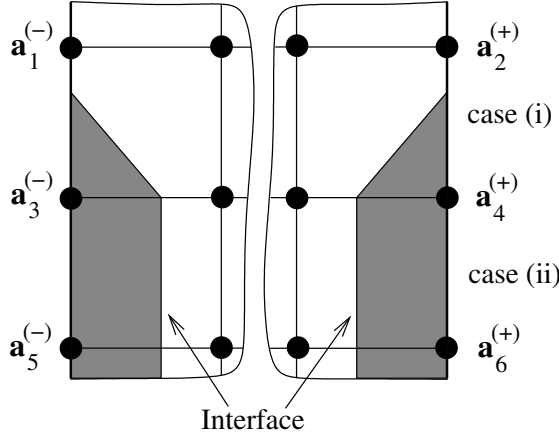


Figure 7: Distinction of different cases regarding the coupling of additional dof

Expressing the periodic boundary conditions based on the displacement field approximation in Eq. (1) shows, that for case (i) the associated dof \mathbf{a} have to be linked. Regarding our example in Fig. 7 we have

$$\begin{aligned} \mathbf{a}_1^{(-)} &= \mathbf{a}_2^{(+)} \quad \text{and} \\ \mathbf{a}_3^{(-)} &= \mathbf{a}_4^{(+)} \quad . \end{aligned} \tag{20}$$

An examination of elements belonging to case (ii) reveals, that the enrichment function becomes $F(\boldsymbol{\xi}) = 0 \quad \forall \quad \boldsymbol{\xi} \in \partial Y$. From this follows, that all additional dof at the unit cell surface of these elements need not to be linked unlike to case (i). Furthermore, since any restrictions regarding these dof will lead to displacement constraints inside the element, no boundary conditions have to be applied at all.

Thus, dof $\mathbf{a}_5^{(-)}$ and $\mathbf{a}_6^{(+)}$ of the mesh example in Fig. 7 remain unchanged. The same applies for the dof $\mathbf{a}_3^{(-)}$ and $\mathbf{a}_4^{(+)}$. However, this requirement conflicts with Eq. (20) where the additional dof of node 3 and 4 are linked. In order to avoid this problem, we have to prevent adjacent X-elements belonging to case (i) and (ii).

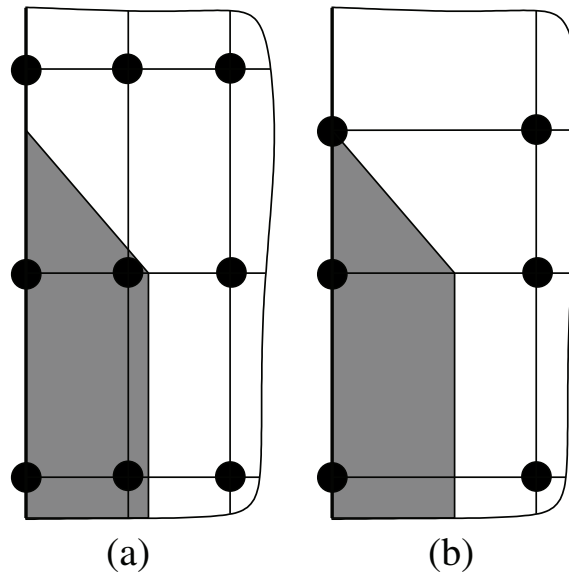


Figure 8: Modification of (a) element sizes and (b) location of element boundaries to avoid incompatible boundary conditions

As illustrated in Fig. 8, this can be achieved by changing the location of element boundaries or smaller element sizes.

5 Application to Textile Reinforced Composites

5.1 Geometry and material properties of the unit cell

Subsequently, the new modelling technique will be applied to the textile reinforced composite material described in Section 1. Before a FE-mesh can be created, the inner geometry of the composite at the meso-scale must be determined. Due to the complex architecture, this requires a detailed analysis which is documented in Haasemann (2008). Thereby, optical and computer tomography scans are used to evaluate predefined geometric parameters. These can be classified into two groups of parameters describing in-plane and out-of-plane distances, respectively. Since the application of a computer tomography is expensive, mathematical dependencies

are developed in order to compute out-of-plane parameters based on the in-plane geometry. After all dimensions are gathered, we can establish a geometric model of the textile reinforcement as shown in Fig. 1. Finally, the FE-mesh of the unit cell at the meso-level based on the combination of X-FEM and Binary Model can be generated (Fig. 9).

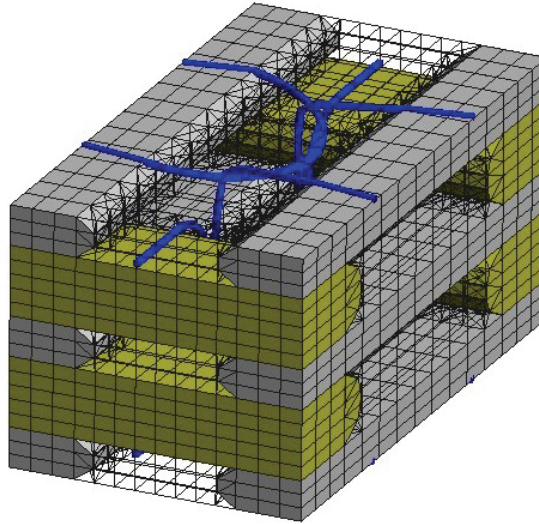


Figure 9: FE-mesh of a unit cell representing a textile reinforced composite

Thereby, all elements representing pure matrix material are set to be transparent. In order to visualise the interfaces of warp- and weft-yarns, the tetrahedra used for integration are shown instead of the entire X-elements. As can be seen in Fig. 9, the biaxial weft-knit in this composite consists of three layers of warp-yarns, two layers of weft-yarns and two systems of weft-knits.

As further requirement, the linear elastic material properties of all composite constituents must be known. One part of the RVE-domain consists of pure matrix material which is an epoxy resin. The Young's modulus ($E_M = 3000\text{MPa}$) and Poisson's ratio ($\nu_M = 0.3$) are determined experimentally.

The remaining RVE-domain is filled with glass fibres saturated by matrix material. Since the weft-knit is represented by line elements, only the axial Young's modulus E_{wk} is required. This can be estimated using the rule-of-mixture

$$E_{wk} = E_m + \nu_{wk}(E_f - E_m) \quad , \quad (21)$$

where the fibre volume fraction is given by $\nu_{wk} = 65\%$. According to Altenbach,

Altenbach, and Rikards (1996), the Young's modulus of glass fibres amounts to $E_f = 78\,000\text{MPa}$.

For modelling the unit cell at the meso-level, all fibre-matrix domains established by warp- and weft-yarns are considered to be homogeneous. Since both groups of domains have nearly the same fibre volume fraction of about $v_{wy} = 60\%$, the small difference is neglected. The homogenisation of a RVE at the micro-level is one possibility to obtain the effective material properties. In order to generate a RVE-model, there are different solutions. According to the fibre distribution in the real composite, a statistically representative volume element can be chosen. However, due to the high modelling effort, it is more efficient to define a unit cell. For this approach, we assume that the effective material behaviour is transversely isotropic.

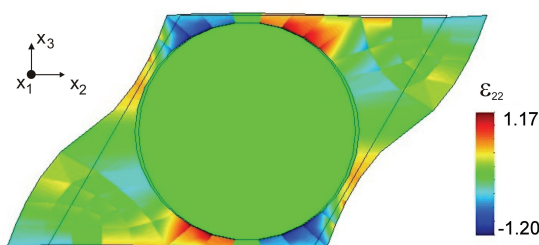


Figure 10: Deformation $E_{22} = 1$ of a microscopic unit cell with $v_W = 60\%$

Then the hexagonal arrangement of fibres results in a unit cell such as shown in Fig. 3. After applying all boundary conditions according to the periodic displacement and anti-periodic traction, six cases of unit deformations have to be solved. One example where $E_{22} = 1$ is shown in Fig. 10. Due to the significant difference between the stiffness of both UD-constituents, the local strain distribution ϵ_{22} inside the fibre domain is nearly zero whereas the remaining matrix domain is subjected to larger deviation from unity. All independent results expressed by engineering constants are summarised in Tab. 2.

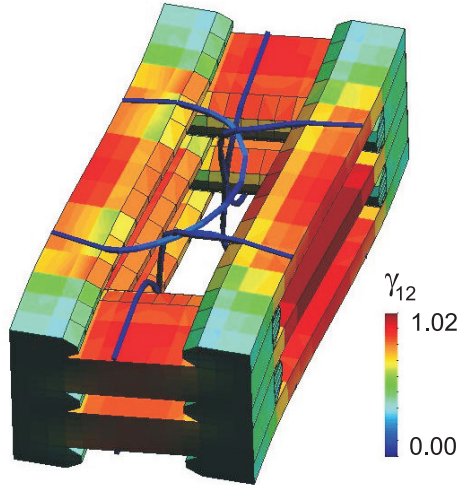
As an alternative to the numerical approach, the elastic material properties can be estimated based on analytical models which have been developed in a broad range. The results of one model which is derived in Skudra, Bulavs, and Rocens (1975) are given in Tab. 2. In comparison to the numerical computation, the analytical elastic parameters represent a material which has a slightly higher stiffness. The influence on the macroscopic material properties of these different results will be investigated in the following section.

Table 2: Material properties of fibre-matrix domain

Engineering parameter	Numerical results	Analytical results
E_1	47 710	48 000
$E_2 = E_3$	10 210	10 960
ν_{23}	0.33	0.41
$\nu_{13} = \nu_{12}$	0.25	0.29
$G_{13} = G_{12}$	4 070	4 410

5.2 Results and verification

As described in Section 4, the computation of macroscopic effective linear elastic material properties requires the simulation of six unit cell deformations. One typical example with $E_{12} = 1$ is shown in Fig. 11.

Figure 11: Deformation $E_{12} = 1$ of the unit cell

Here again, for a better view inside the unit cell, the domain of pure matrix material is transparent. The colour scale in Fig. 11 represents the local shear strain γ_{12} . According to the macroscopic strain, the local distribution is dominated by $\gamma_{12} \approx 1$. In order to verify the numerical results, experimental tests have been performed.

As documented in Haasemann (2008), the analysis of test data obtained by tensile, bending and shear tests provides a complete characterisation of the elastic in-plane properties.

The comparison of in-plane Young's modulus $E(\alpha)$ and Poisson's ratio $\nu(\alpha)$ depending on the textile orientation α are shown in Fig. 12 and 13.

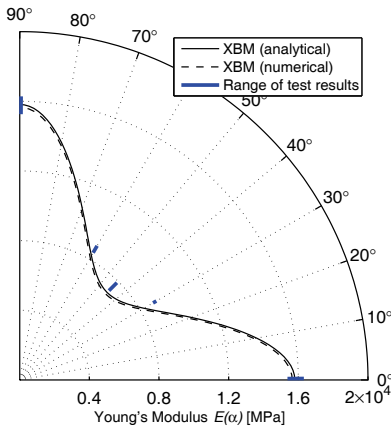


Figure 12: Polar diagram of in-plane Young's modulus

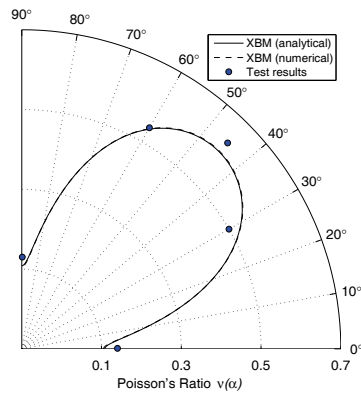


Figure 13: Polar diagram of in-plane Poisson's ratio

Here it is assumed that $\alpha = 0$ corresponds to the warp-yarn orientation. The results based on the numerical and analytical approach described in Section 5.1 to compute the effective material properties of the yarn-matrix domain are represented in both polar plots by solid and dashed lines, respectively. Thereby it can be seen, that there is no significant difference between the homogenised results.

In the following we will summarise some general elastic properties of the composite based on these two polar plots. Since the fibre volume fraction related to the unit cell of warp- and weft-yarn are equal, there is almost no deviation between $E(0^\circ)$ and $E(90^\circ)$. The same applies to $\nu(0^\circ)$ and $\nu(90^\circ)$. The curve of the Young's modulus is characterised by a significant drop around 45° which is due to the absence of any yarn in this direction. Furthermore, the Poisson's ratio at 0° and 90° is quite small. This is caused by the straight warp- and weft-yarns which obstruct the Poisson's effect.

Comparing numerical and experimental results we find a good agreement which emphasises the quality of the proposed modelling technique. The reason for small deviation may be found by considering the influence of technological aspects and internal stresses.

6 Conclusions

This paper has presented a new modelling technique based on the combination of X-FEM and Binary Model. It is especially developed for the efficient generation of FE-meshes representing the inner architecture of textile reinforced composites. The approach utilises its main advantages with the application to biaxial weft-knit reinforcement. Thereby, regular shaped elements based on the X-FEM represent the material interface between pure matrix material and yarn-matrix domains while the weft-knit is modelled with line elements. So the element size of the underlying base mesh does not depend on the small cross-section given by the weft-knit.

The application of the new modelling technique in this paper is focused on the computation of effective material properties based on homogenisation techniques. As it was shown, the use of periodic displacement boundary conditions in conjunction with elements based on the X-FEM requires special considerations. For this, different cases for the formulation of constraints regarding additional dof are analysed.

Finally, the combination of X-FEM and Binary Model is applied to a particular composite with biaxial weft-knit reinforcement. There, a good agreement of numerical and experimental results is obtained and proves the ability of this new modelling technique.

Acknowledgement: The work done for this paper is sponsored by the German Research Community (DFG) in the context of the collaborative research center (SFB) no. 639.

References

Altenbach, H.; Altenbach, J.; Rikards, R. (1996): *Einführung in die Mechanik der Laminat- und Sandwichtragwerke*. Deutscher Verlag für Grundstoffindustrie Stuttgart.

Carter, W.; Cox, B.; Fleck, N. (1994): A binary model of textile composites - I. Formulation. *Acta. metall. mater.*, vol. 42, no. 10, pp. 3463–3479.

Chirputkar, S. U.; Qian, D. (2008): Coupled atomistic/continuum simulation based on extended space-time finite element method. *CMES: Computer Modeling in Engineering & Sciences*, vol. 24, no. 3, pp. 185–202.

Cox, B.; Dadkhah, M. (1995): The macroscopic elasticity of 3D woven composites. *J. Compos. Mater.*, vol. 29, no. 6, pp. 785–819.

Dang, T. D.; Sankar, B. V. (2008): Meshless local Petrov-Galerkin micromechanical analysis of periodic composites including shear loadings. *CMES: Computer Modeling in Engineering & Sciences*, vol. 26, no. 3, pp. 169–187.

Galli, M.; Botsis, J.; Janczak-Rusch, J. (2008): An elastoplastic three-dimensional homogenization model for particle reinforced composites. *Comp. Mater. Sci.*, vol. 41, no. 3, pp. 312–321.

Haasemann, G. (2003): An application of the binary model to dynamic finite element analysis. *Proc. Appl. Math. Mech.*, vol. 3, no. 1, pp. 176–177.

Haasemann, G. (2008): *Effektive mechanische Eigenschaften von Verbundwerkstoffen mit Biaxialgestrickverstärkung*. PhD thesis, TU Dresden, 2008. TUDpress, ISBN 978-3-941298-01-9.

Haasemann, G.; Kästner, M.; Ulbricht, V. (2006): Multi-scale modelling and simulation of textile reinforced materials. *CMC: Computers, Materials & Continua*, vol. 3, no. 3, pp. 131–146.

Hagihara, S.; Tsunori, M.; Ikeda, T.; Miyazaki, N. (2007): Application of meshfree method to elastic-plastic fracture mechanics parameter analysis. *CMES: Computer Modeling in Engineering & Sciences*, vol. 17, no. 2, pp. 63–72.

Hill, R. (1963): Elastic properties of reinforced solids: Some theoretical principles. *Journal of the Mechanics and Physics of Solids*, vol. 11, no. 5, pp. 357–372.

Hollister, S. J.; Kikuchi, N. (1992): A comparison of homogenization and standard mechanics analyses for periodic porous composites. *Computational Mechanics*, vol. 10, no. 2, pp. 73–95.

Huang, S.-J.; Chiu, L.-W. (2008): Modeling of structural sandwich plates with 'through-the-thickness' inserts: Five-layer theory. *CMES: Computer Modeling in Engineering & Sciences*, vol. 34, no. 1, pp. 1–32.

Kästner, M.; Haasemann, G.; Brummund, J.; Ulbricht, V. (2008): *Computation of effective stiffness properties for textile-reinforced composites using X-FEM*, chapter 13, pp. 261–279. Springer, 2008.

Kästner, M.; Ulbricht, V. (2006): Homogenization of fibre composites using X-FEM. *Proc. Appl. Math. Mech.*, vol. 6, no. 1, pp. 489–490.

Liu, D.; Chen, C.; Chiou, D. (2005): 3-d modeling of a composite material reinforced with multiple thickly coated particles using the infinite element method. *CMES: Computer Modeling in Engineering & Sciences*, vol. 9, no. 2, pp. 179–192.

Long, S.; Liu, K.; Li, G. (2008): An analysis for the elasto-plastic fracture problem by the meshless local Petrov-Galerkin method. *CMES: Computer Modeling in Engineering & Sciences*, vol. 28, no. 3, pp. 203–216.

McGlockton, M.; Cox, B.; McMeeking, R. (2003): A binary model of textile composites: III. high failure strain and work of fracture in 3D weaves. *J. Mech. Phys. Solids.*, vol. 51, no. 8, pp. 1573–1600.

Melenk, J. M.; Babuska, I. (1996): The partition of unity finite element method: Basic theory and applications. *Computer Methods in Applied Mechanics and Engineering*, vol. 139, no. 1-4, pp. 289–314.

Moës, N.; Cloirec, M.; Cartraud, P.; Remacle, J.-F. (2003): A computational approach to handle complex microstructure geometries. *Comput. Method. Appl. M.*, vol. 192, pp. 3163–3177.

Moës, N.; Dolbow, J.; T., B. (1999): A finite element method for crack growth without remeshing. *Int. J. Numer. Meth. Engng.*, vol. 46, pp. 131–150.

Pahr, D. H.; Böhm, H. (2008): Assessment of mixed uniform boundary conditions for predicting the mechanical behavior of elastic and inelastic discontinuously reinforced composites. *CMES: Computer Modeling in Engineering & Sciences*, vol. 24, no. 2, pp. 117–136.

Pierard, O. (2006): *Micromechanics of inclusion-reinforced composites in elasto-plasticity and elasto-viscoplasticity: modeling and computation*. PhD thesis, Université Catholique de Louvain, 2006.

Rolfes, R.; Ernst, G.; Hartung, D.; Teßmer, J. (2006): Strength of textile composites - a voxel based continuum damage mechanics approach. In *Computational Mechanics: Solids, Structures and Coupled Problems*, pp. 497–520. Springer.

Skudra, A.; Bulavs, F.; Rocens, K. (1975): *Kriechen und Zeitstandverhalten verstärkter Plaste*. VEB Deutscher Verlag für Grundstoffindustrie.

Stazi, F.; Budyn, E.; Chessa, J.; Belytschko, T. (2003): An extended finite element method with higher-order elements for curved cracks. *Comp. Mech.*, vol. 31, no. 1-2, pp. 38–48.

Takashima, S.; Nakagaki, M.; Miyazaki, N. (2007): An elastic-plastic constitutive equation taking account of particle size and its application to a homogenized finite element analysis of a composite material. *CMES: Computer Modeling in Engineering & Sciences*, vol. 20, no. 3, pp. 193–202.

Ulbricht, V.; Kästner, M.; Lichtneckert, T.; Brummund, J.; Modler, K.-H.; Hufenbach, W.; Böhm, R.; Ebert, C.; Grüber, B.; Langkamp, A.; Lepper, M. (2008): Modelling of the effective material behavior of textile reinforced composites. *Journal of Plastics Technology*, vol. 4, pp. 1–30.

Wang, S.; Lim, K.; Khoo, B.; Wang, M. (2007): A geometric deformation constrained level set method for structural shape and topology optimization. *CMES: Computer Modeling in Engineering & Sciences*, vol. 18, no. 3, pp. 155–181.

Xu, J.; Cox, B.; McGlockton, M.; Carter, W. (1995): A binary model of textile composites–II. The elastic regime. *Acta Metallurgica et Materialia*, vol. 43, no. 9, pp. 3511–3524.